Optical and Quantum Electronics (2021) 53:354
https://doi.org/10.1007/s11082-021-03024-5

A novel multi-band biomedical sensor for THz regime

Aruna Veeraselvam[1] · Gulam Nabi Alsath Mohammed[1] · Kirubaveni Savarimuthu[1] · Radha Sankararajan[1]

Received: 17 April 2021 / Accepted: 8 June 2021 / Published online: 29 June 2021

Abstract
This paper presents the design and evaluation of a multi-band terahertz (THz) metamaterial-based biomedical (BioMed) sensor for blood component detection such as Deoxyribonucleic acid (DNA), Ribonucleic acid (RNA), plasma, water, Red Blood Cells (RBC), White Blood Cells (WBC) and haemoglobin. The proposed THz sensor is a multimode resonator with concentric square loops enclosing concentric octagonal loops. The proposed sensor has a metamaterial feature with a footprint of $0.164\lambda_{eff} \times 0.164\lambda_{eff}$. The THz sensor operates between 1 and 2 THz with four independently tunable operating bands, viz. 0.33, 0.90, 1.42 and 1.85 THz. The sensitivity of the THz sensor is estimated using the absorption characteristics, and the estimated average absorptivity is 99% for the proposed BioMed sensor. The THz sensor has a rotational symmetry offering both polarization and angular stability (up to 60°). The performance of the sensor is evaluated for different BioMed samples providing unique refractive indices. Furthermore, the impact of sample thickness on the sensor performance has been evaluated and presented. From the results, it is inferred that the proposed THz sensor is suitable for nucleic acids and other components detection in blood samples.

Keywords THz sensors · Metamaterials · Biomedical sensor · THz imaging

1 Introduction

Blood is a vital entity for life in the universe. The blood is a complex mixture of water and various cells that transport oxygen to key organs in a biological system. The pathogen infection of the blood is found by variation in its components such as RBC, WBC, plasma, water, nucleolus, and nucleic acids such as RNA and DNA. Detection of those components serves as an important means of disease diagnosis and treatment. Recently, there is a surge of research interest in using THz radiation for diagnostic applications (Emami Nejad et al. 2019). When the blood sample is exposed to radiation, the amount of radiation absorbed provides information about the constituents present in the sample.

✉ Gulam Nabi Alsath Mohammed
gulamnabialsathm@ssn.edu.in

[1] Department of Electronics and Communication Engineering, Sri Sivasubramaniya Nadar College of Engineering, Kalavakkam, Chennai 603 110, India

Terahertz frequencies have less energy compared to higher frequencies in the electromagnetic spectrum. Lesser energy makes the THz waves non-invasive and hence less harmful for practical implementation. Since THz radiations are non-ionizing, they serve to be a safer choice for diagnostics as compared to the existing techniques like X-rays. Metamaterial structures at THz frequencies enabled researchers to develop many novel miniaturized components and devices, which offer independent tunability of permittivity, permeability, and index of refraction. The negative properties of the metamaterial result in the development of low-loss resonant structures for highly accurate THz sensors for BioMed applications. This research focuses on the development of one such sensor that can be deployed for sensing and imaging based on the amount of radiation it has absorbed. The performance of the sensor can be evaluated using the reflection, transmission, and absorption characteristics. In this research, the absorption property of the metamaterial sensor is used as a means to evaluate the performance of the proposed BioMed sensor.

In literature, several studies have been reported in the development of novel THz metamaterials as absorbers. The use of THz metamaterial in spectroscopic imaging has been extensively described in Sanphuang et al. (2015) and MacPherson et al. (2013). The performance of the THz metamaterial sensor greatly depends on the choice of materials such as gold (Al-Naib 2017) and graphene (He and Chen 2013). In (Wang 2018), the researchers have evaluated the conductivity of thin films used in THz frequencies. State-of-the-art research involves the development of THz metamaterials with a single band, broadband, and multi-band characteristics. A brief review of each of the techniques has been described.

A polarization-insensitive perfect metamaterial absorber is realized using a split ring resonator by Landy et al. (2008). In (Butler et al. 2011) an electric ring resonator is designed at 0.84 THz with absorptivity 99.6% and the same research has been extended and investigated in Wilbert et al. (2013) with an equivalent circuit for polarization instability. In (Landy et al. 2009), the authors have realized a complicated dual-layer absorber with a cross structure on one layer and a four-fold resonator with rotational symmetry on another layer. The reported absorber has a footprint of $0.675\lambda_{eff} \times 0.675\lambda_{eff}$ and resonates at 1.13 THz with 95% absorptivity. The λ_{eff} is the effective wavelength calculated at the lowest resonance frequency. The study of single-band characteristics is followed by analyzing the broadband characteristics of terahertz absorbers in He and Chen (2013). Similarly, a broadband absorber with polarization insensitivity is designed in Wang et al. (2018). Specifically, the interference and diffraction effects of the broadband absorber is reported in Shi (2016). A dual-band absorber is designed in Wang et al. (2015) using an asymmetric patch that operates at 1.72 and 1.90 THz. A tri-band plus-shaped metamaterial absorber is designed in Elakkiya et al. (2019) with a peak absorption of 98% at 0.4728 THz. A # shaped perfect metamaterial absorber is presented in Hu et al. (2016) with a unit cell size of $0.437\lambda_{eff} \times 0.437\lambda_{eff}$ and the absorber offers four absorption bands. Similarly, a quad-band asymmetric metamaterial absorber with $0.299\ \lambda_{eff} \times 0.299\lambda_{eff}$ is reported in Wang and Wang (2016). In (Wang and Wang 2015), a pentaband comb resonator of size $0.287\ \lambda_{eff} \times 0.287\ \lambda_{eff}$ is reported with absorption greater than 98%. A five-band nested split ring resonator is designed in Wang et al. (2016), whose unit cell size is $0.292\lambda_{eff} \times 0.292\lambda_{eff}$ produces an average peak absorption of 99% between 0.5 to 3 THz. Thus, the metamaterial absorbers have received considerable research attention in the THz component development.

In line with this, the state-of-the-art in THz component development has been extended to the design of sensors for BioMed applications. The researchers in Failed (2002) have presented a THz biomolecular sensor for DNA detection using the refractive index property of the genetic material. In (Ahmed 2019), the authors proposed a compact cladding

photonic crystal fibre (CC-PCF) with five distinct operating bands for blood component detection with a sensitivity greater than 80%. A graphene plasmonic sensor is reported in Nejat and Nozhat (2019) with a single absorption peak. The reported sensor has been demonstrated for blood glucose detection and to perform disease characterization by estimating the refractive index changes. A split-ring resonator (SRR) based THz BioMed sensor operating at 2.249 THz is reported in Saadeldin et al. (2019) with a sensitivity of 300 GHz/refractive index unit (RIU). In recent years, the researchers show a great interest in designing multi-band sensors rather than single narrowband or broadband sensors as they are limited by poor sensitivity and low resolution. Multiband sensors are desirable for BioMed applications due to their high resolution and good accuracy (Ansari et al. 2018; Nejat and Nozhat 2020). Thus, in this paper, a quad-band THz metamaterial sensor is designed and analyzed for BioMed applications. From the literature, it is inferred that designing multi-band sensor with high absorption and independent frequency control is a challenging task. Therefore, this paper proposes a BioMed sensor operating at four distinct frequency bands between 0.1 to 2 THz with smaller size and high absorption characteristics. The estimated average absorptivity is 99.25% for the proposed quad-band sensor. The theoretical values of the refractive index of biological samples are used to estimate the sensitivity of the proposed THz sensor. The rest of the manuscript is organized as follows. Section II of the manuscript presents the design and characterization of the proposed THz sensor. Section III details the parametric analysis, polarization and angular stability characteristics. The sensitivity analysis of the proposed sensor is discussed in Section IV. The simulation of the proposed THz sensor is performed using Computer Simulation Technology (CST) Studio Suite 2018 (www.3ds.com) employing Finite Integration Technique (FIT) as an electromagnetic computational method. FIT uses maxwell's equation in their integral form to prove the conservation properties of the discrete fields before calculating numerically. This computation method is used to analyze the absorptivity, sensitivity, full width half maximum and figure of merit of THz sensor.

2 Terahertz sensor design

2.1 Construction

The geometry of the proposed THz BioMed sensor is shown in Fig. 1. The proposed sensor senses the variation in the absorption characteristics when exposed to the analyte under investigation. The geometrical details of the proposed sensor are described in Fig. 1a. The side view and the perspective view of the THz sensor are described in Fig. 1b, c respectively. The unit cell metamaterial sensor has a footprint of 80 µm (L) × 80 µm (W) and is synthesized on a lossy silicon wafer of thickness, $h_1 = 50$ µm. The silicon wafer is decoupled from the polyimide substrate using a 0.5 µm (h_3) thin ground copper layer. Hence, the silicon wafer does not alter the electrical characteristics of the proposed sensor offering only the desired mechanical strength to the sensor. Further, the sandwiched ground layer prevents the transmittance of electromagnetic radiation thereby improving the absorption characteristics. The frequency-dependent metallic patterns of the sensor are etched over an 18 µm (h_2) thin polyimide substrate with permittivity of 3.5 and loss tangent 0.0027. The metallic patterns are created using 0.5 µm (h_4) thin copper (Cu) with frequency-independent conductivity of 5.96×10^7 S/m. The thickness of the copper metal patterned is optimized to 0.5 µm since the skin depth is 0.2 µm and lesser for frequencies above 0.1 THz.

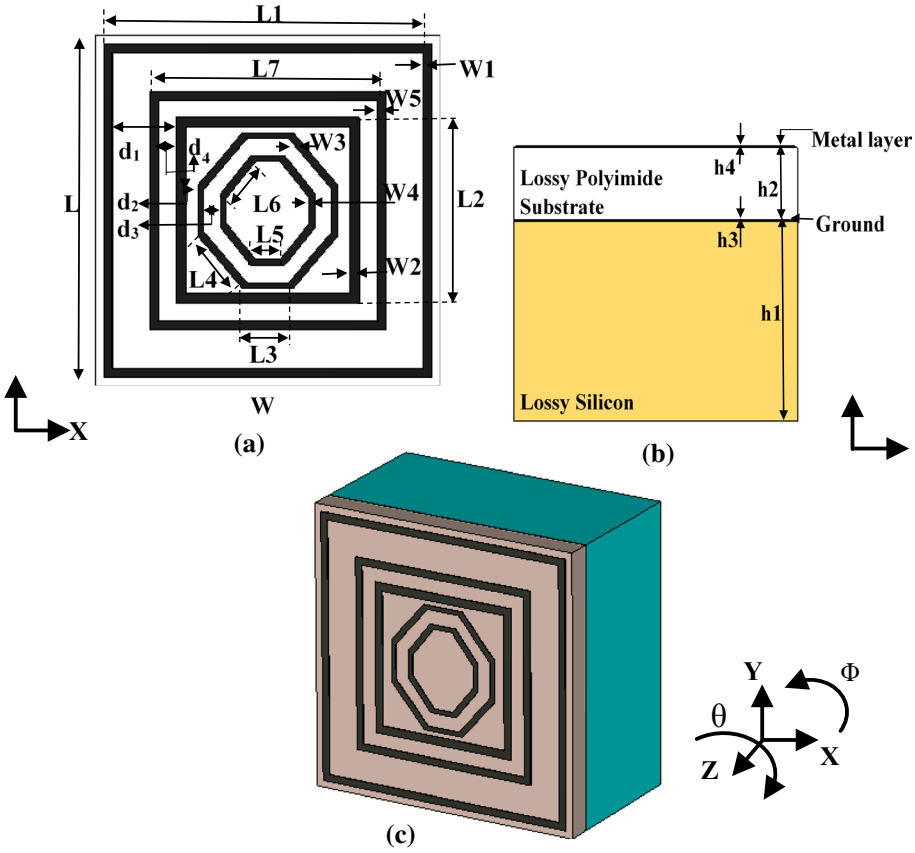

Fig. 1 Proposed unit cell sensor. **a** Top view. **b** Side view. **c** Perspective view

The characteristics of the proposed THz sensor are analyzed using the Floquet mode theory with periodic boundary conditions along 'x' and 'y' directions. The proposed sensor is excited by THz radiation along the 'z' direction. The scattering parameters are used to derive the absorption properties of the proposed sensor. The absorptivity or the absorbed power is estimated using Eq. (1) (Landy et al. 2008).

$$A(\omega) = 1 - R(\omega) - T(\omega) = 1 - |S_{11}|^2 - |S_{21}|^2 \tag{1}$$

where $|S_{11}|$ is the reflection coefficient and $|S_{21}|$ is the transmission coefficient. $T(\omega) = |S_{21}| = 0$ due to the copper layer beneath the polyimide substrate. Thus, Eq. (1) reduces to Eq. (2) (Elakkiya et al. 2019) as given below.

$$A(\omega) = 1 - R(\omega) = 1 - |S_{11}|^2. \tag{2}$$

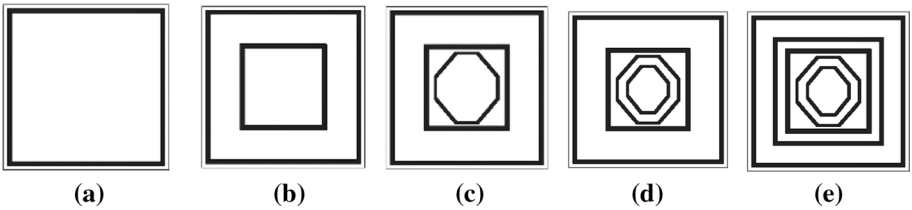

Fig. 2 Evolution of the proposed THz sensor. **a** Resonator 1. **b** Resonator 2. **c** Resonator 3. **d** Resonator 4. **e** Proposed resonator

Fig. 3 Absorption characteristics at different stages of evolution

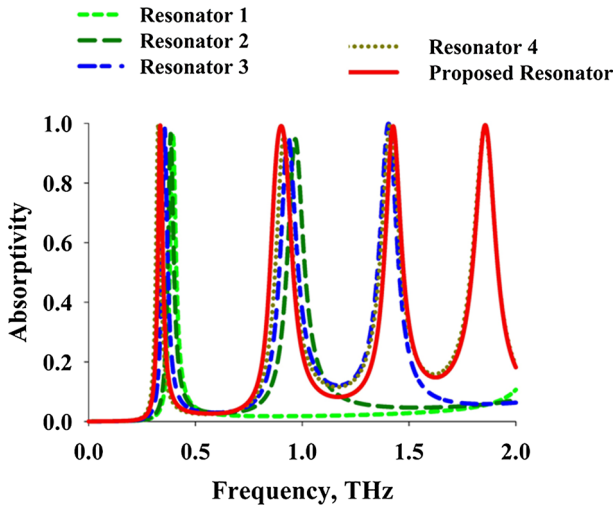

2.2 Evolution

The evolution of the proposed THz sensor and the corresponding absorption characteristics are plotted in Figs. 2 and 3 respectively. The proposed THz sensor evolved from a square loop of side length $L_1 = 77$ μm at the periphery of the sensor corresponding to the lower resonant frequency of 0.39 THz. This square loop offers 96% absorptivity at the intended frequency. To this resonator, a concentric square loop of side length $L_2 = 52$ μm is added as illustrated in Fig. 2b. The two square loops are separated by the distance of $d_1 = 12.5$ μm. At this design stage, resonator 2 offers a dual-frequency response at 0.39 THz and 0.97 THz with an absorptivity of 95%. To further increase the number of resonances, two coupled octagonal resonators are enclosed within the square resonators as described in Fig. 2c, d. The optimized total length of the outer and inner concentric octagonal loops is 144 μm and 112 μm respectively to obtain resonance at 1.41 and 1.85 THz respectively. The distance between the two concentric octagonal loops is fixed as $d_3 = 4.5$ μm. The resonator 4 in Fig. 2d offers four absorption peaks with absorptivity greater than 98% except for the second absorption peak. To improve the absorption performance at the second frequency, the inner square loop in Fig. 2d is replaced by a coupled square resonator as described in Fig. 2e. The addition of the square loop with the resonator shown in Fig. 2d improves the absorptivity of the second

band from 95 to 100%. This specific modification has resulted in the implementation of coupled square loops and coupled octagonal loops encompassed inside the outermost square loop.

The optimization of the different parameters is conducted using the particle swarm optimization (PSO) technique in CST and is consolidated in Table 1. The optimization is carried out by varying one parameter while fixing the other parameters. During optimization, the target was to obtain peak absorptivity in all four frequency bands. The optimized parameters of the proposed THz sensor are given in Table 2. Figure 4 illustrates the reflection ($|S_{11}|$), transmission ($|S_{21}|$) and absorption properties of the proposed micro-resonator. From the figure, it can be inferred that the proposed sensor has zero transmission characteristics, a very low reflection property, and extremely

Table 1 Optimization parameters of the proposed THz sensor

Sl. no.	Optimization parameter	Range (μm)	Optimum value (μm)
1	L1	76–78	77
2	L2	52–56	54
3	L3	15–17	16
4	L4	18–19.25	18.75
5	L5	10–11.25	10.75
6	S1	136–152	144
7	S2	113–122	118

Table 2 Optimized dimension of the proposed THz sensor

Parameter	L	W	L1	L2	L3	L4	L5	L6	L7	W1	W2
Value (μm)	80	80	77	52	16	20	10	18	54	0.1	0.2
Parameter	W3	W4	W5	d1	d2	d3	d4	h1	h2	h3	h4
Value (μm)	0.3	0.5	0.3	12.5	2	4.5	1	50	18	0.5	0.5

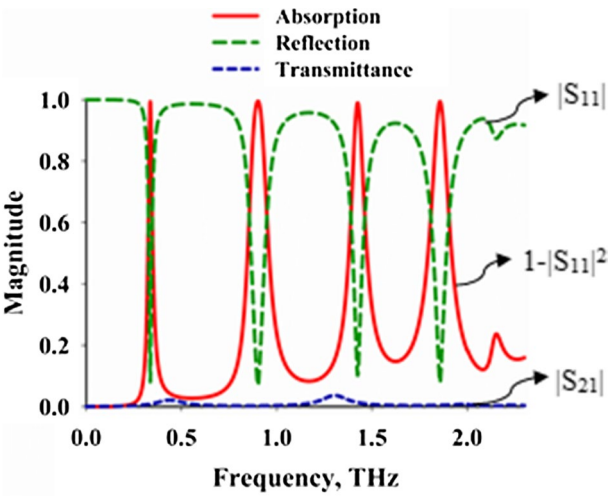

Fig. 4 Reflection, transmittance, and absorption characteristics of the proposed THz sensor

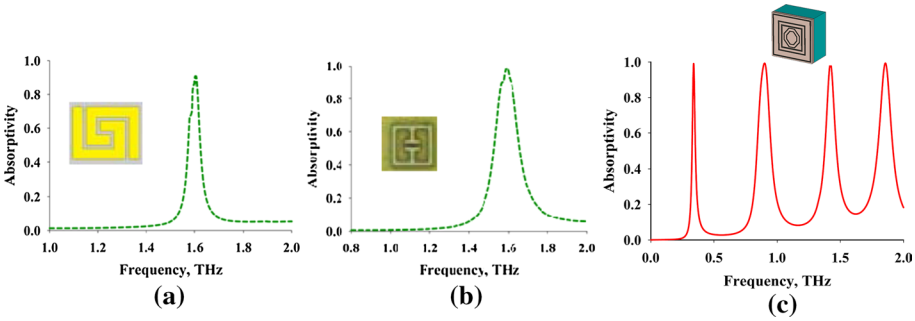

Fig. 5 Absorption characteristics in the author's simulation window for **a** Spiral absorber (Saadeldin et al. 2019), **b** Split ring resonator (Primo and Lebars 2007), **c** Proposed sensor

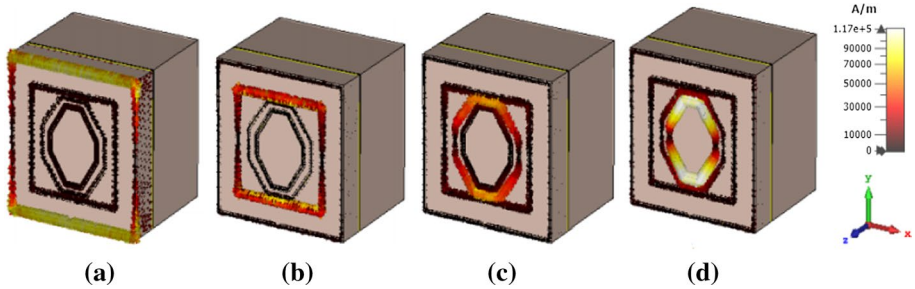

Fig. 6 Surface plasmon distribution at **a** 0.33 THz, **b** 0.90 THz, **c** 1.42 THz, and **d** 1.85 THz

high absorptivity at the four design frequencies, viz. 0.33, 0.90, 1.42 and 1.85 THz with absorptivity 99%, 100%, 99% and 99% respectively.

Furthermore, the accuracy of the numerical calculations is verified by repeating the exercises proposed in Saadeldin et al. (2019) and (Tao 2008). The authors in Saadeldin et al. (2019) used the full vectorial finite element method and they have proved their accuracy by reproducing the results in Tao et al. (2008). In line with this, the authors have simulated the designs in Tao et al. (2008) and (Saadeldin et al. 2019). This accuracy is met by fixing the number of mesh lines per wavelength as 15 and simulation accuracy is set to 10^{-6} in the frequency domain solver of CST. The smallest mesh cell size is 0.155 μm while the minimum element quality is 0.00357. Figure 5a–c shows the absorption characteristics of Saadeldin et al. (2019); Tao et al. 2008) and the proposed sensor respectively. From the figures, it can be inferred that the proposed biosensor can work in line with the research presented in Saadeldin et al. (2019) and (Tao et al. 2008). From the results, it can be inferred that the multi-band nature of the THz sensor will be retained thus guarantying the performance against fabrication tolerance.

2.3 Surface plasmon effects

The surface plasmon distribution of the proposed sensor is plotted in Fig. 6 to further validate the influence of the multi-loop resonator on the absorption characteristics. The plasmons are more concentrated around the outer loop for the lowest absorption

frequency of 0.33 THz as shown in Fig. 6a. The current density is found high around the coupled square resonator (Fig. 6b) and octagonal resonators (Fig. 6c–d) at 0.9, 1.42, and 1.85 THz respectively indicating the impact of these resonators at the second, third and fourth absorption bands. Thus, the proposed THz sensor lacks surface hybridizations resulting in independent control of the absorption peaks.

2.4 Parametric analysis

The sensitivity of the THz sensor is estimated using the absorption characteristics of the proposed sensor. The absorptivity is influenced by the geometrical parameters used in the design of the THz sensor. Among the various parameters, the length of the square resonator (L1), length of the outer concentric square loop (L_2), the total length of the coupled octagonal loops (S_1 & S_2), and thickness of the substrate (h_2) are varied to validate the resonant bands that are independently controlled by the parameters. The length of the outer square L1 is varied from 76 to 78 µm. L1 shows a strong influence on the lower absorption peak as described in Fig. 7. The absorption peak shifts towards the low frequency with an increase in the side length L1. The estimated tunability is 64 GHz/µm.

Similarly, the influence of L2 on the second absorption peak is evaluated and presented in Fig. 8. From the figure, it is inferred that mode splitting occurs for values of L2 greater than 56 µm while the absorptivity decreases for L2 less than 52 µm. Hence L2 can be varied between 52 and 56 µm and the estimated tunability is 30 GHz/µm. The impact of the lengths of outer and inner octagonal loops are evaluated and presented in Figs. 9 and 10 respectively. The tunability at the third and fourth absorption peaks are estimated to be 3.3 GHz/µm and 10 GHz/µm respectively. Further analysis is made to determine the impact of polyimide thickness on the absorption characteristics of the proposed sensor and the characteristics are plotted in Fig. 11. From the figure, it can be inferred that the thickness of the substrate has a negligible impact on the absorption frequencies of the proposed sensor.

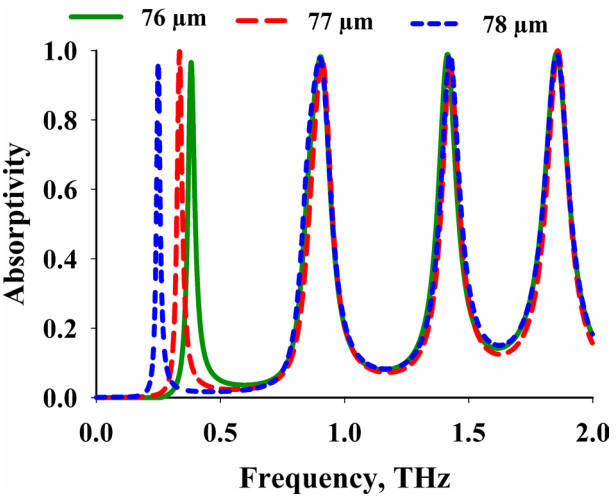

Fig. 7 Impact of the length of outer square (L_1) on the proposed THz sensor

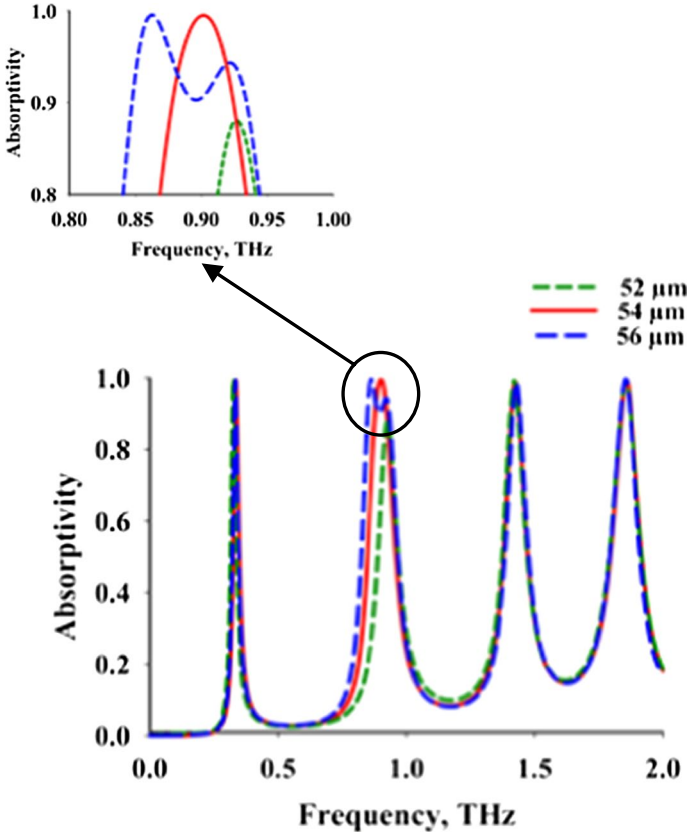

Fig. 8 Effect of length of the outer coupled square loop (L_2) on absorptivity

2.5 Influence of conductors

This section presents the absorption performance of the THz sensor for different conductors that can be used for developing the sensor. Copper with a conductivity of 5.96×10^7 S/m is used during the initial design stage. Also, Gold and Platinum with frequency-independent conductivity of 4.56×10^7 S/m and 9.52×10^7 S/m respectively are chosen to analyze the impact of conductivity on the absorption characteristics. Figure 12 illustrates the absorption characteristics of different conductors. From the figure, it can be inferred that Platinum shows relatively inferior performance (10% reduction in the absorptivity) compared to Gold and Copper. The performance of the sensor using Gold and Copper shows nearly identical characteristics. In addition to this, the loss performance of the THz sensor is evaluated and presented in Fig. 13. From the results, it can be inferred that the ohmic loss characteristics of the metal provide the desired absorption characteristics. The absorption performance is lost under ideal conditions of the metal. The lossy nature of the polyimide substrate has a negligible influence on the absorption characteristics as described in Fig. 13.

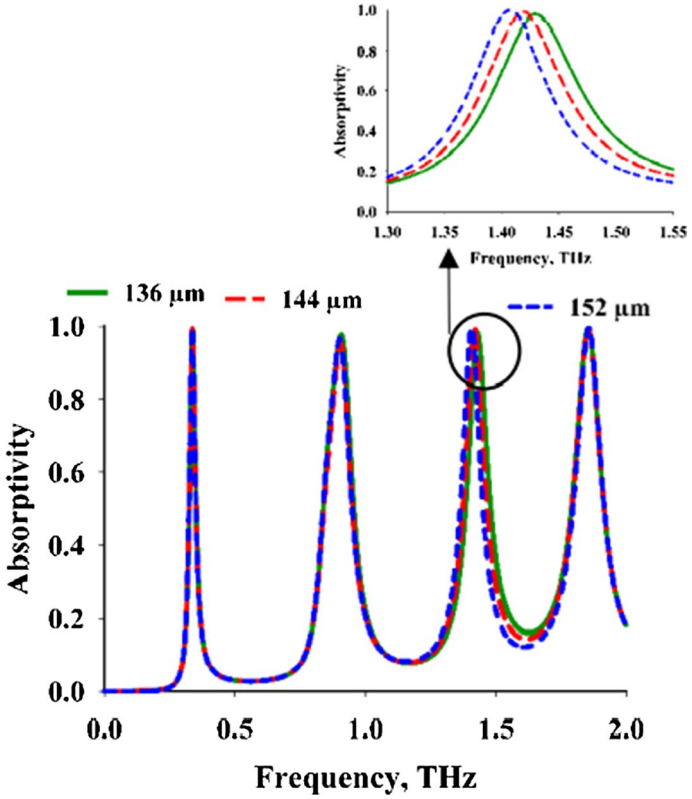

Fig. 9 Effect of length of the outer octagonal loop (S1 = 4*L3 + 4*L4) on absorptivity

3 Stability analysis

The polarization and angular stability of the proposed THz sensor are evaluated and presented in this section. The sensor is subject to THz radiation along the 'z' direction. Transverse Electric (TE) and transverse magnetic (TM) modes of propagation are used for evaluating the polarization stability by varying $\phi = 0°$ and 90° under normal incidence ($\theta = 0°$) case. The proposed THz sensor has a rotational geometry and hence TE mode of operation is identical to the TM mode of operation as shown in Fig. 14. Hence, it is evident that the absorption spectra are stable for both TE and TM mode. Thus, the proposed sensor is polarization insensitive.

Furthermore, the influence of the EM waves with oblique incidence on the absorption characteristics is studied and presented in Fig. 15. The angular stability is measured as the range of angles (θ) over which the sensor is estimated to exhibit identical characteristics. Thus, the proposed THz sensor is angularly independent for $\theta = 60°$. Since the proposed THz sensor is polarization independent, the oblique incidence case for both TE and TM modes of propagation are identical. Hence it can be concluded that the proposed sensor is insensitive to both polarization and angular variations.

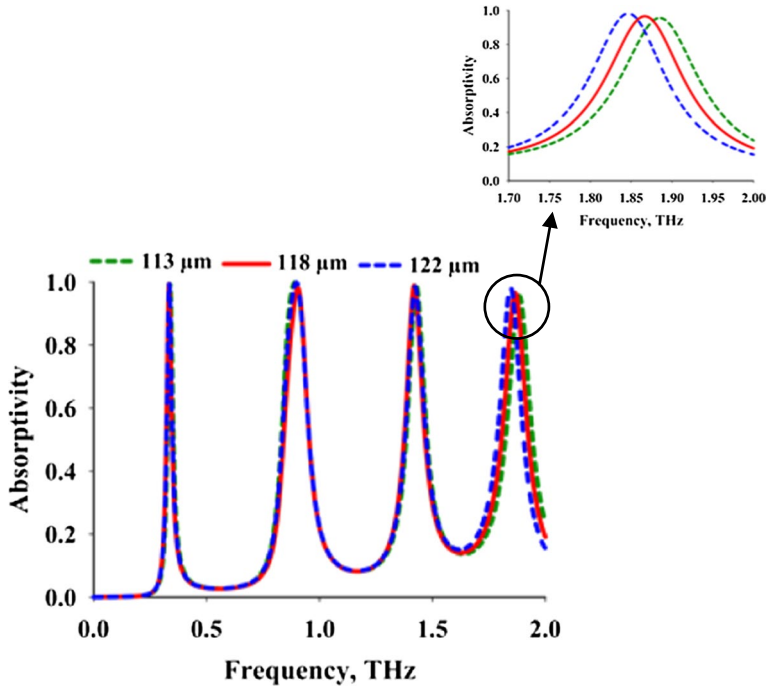

Fig. 10 Effect of the length of the outer octagonal loop (S2 = 4*L5 + 4*L6) on absorptivity

Fig. 11 Effect of the thickness of the substrate (h_2) on absorptivity

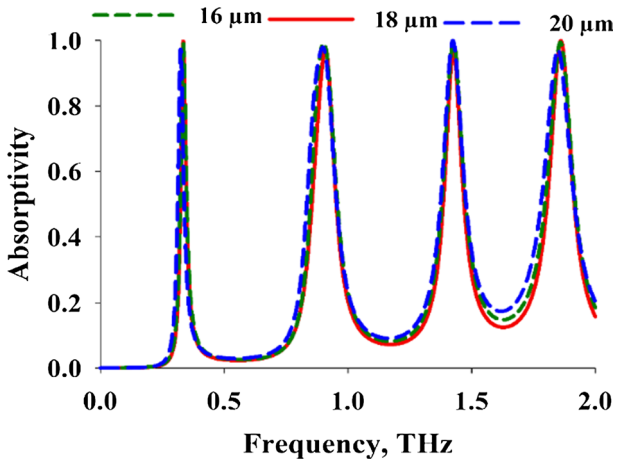

4 Sensitivity estimation

In this section, the suitability of the proposed THz sensor for BioMed applications has been evaluated and presented. More specifically, the detection of the blood cell components using the THz sensor has been attempted, and the results are discussed. The sensitivity of the THz sensor for various components in the blood is systematically studied

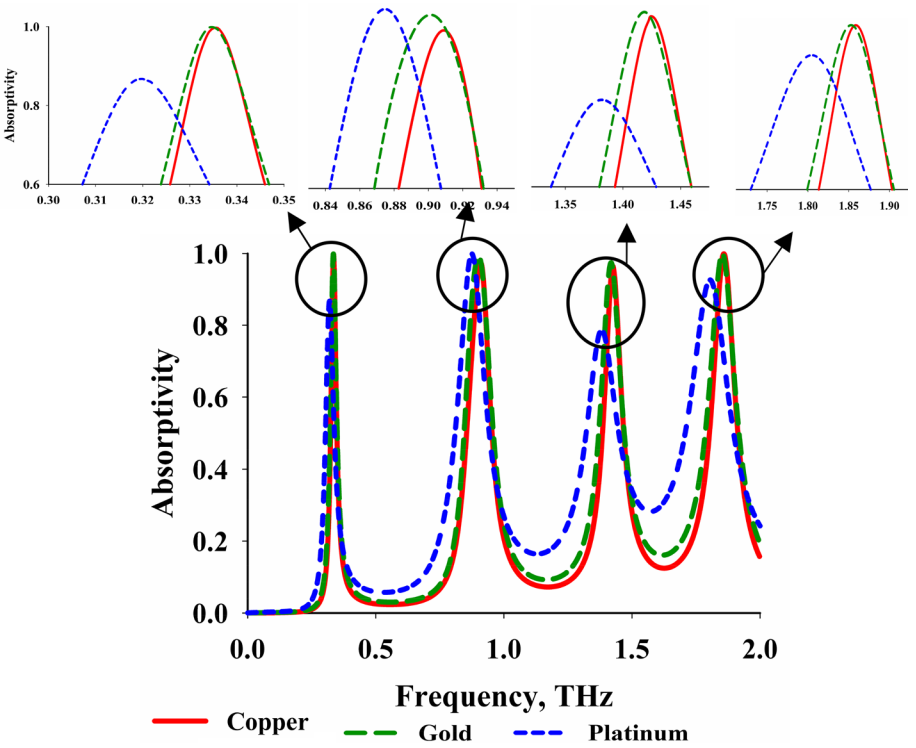

Fig. 12 Absorption characteristics for different metal layers

Fig. 13 Loss performance of the proposed THz sensor

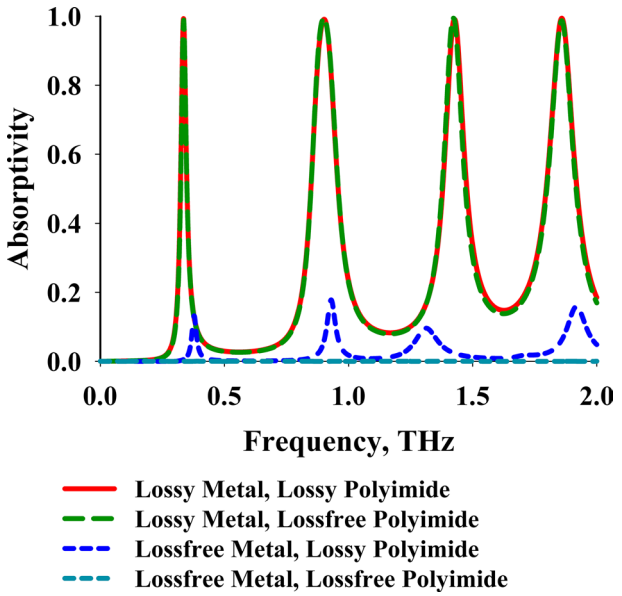

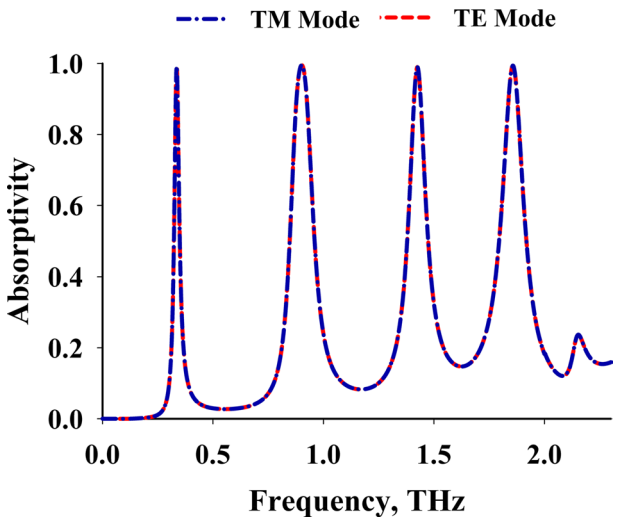

Fig. 14 Polarization stability characteristics of the proposed sensor

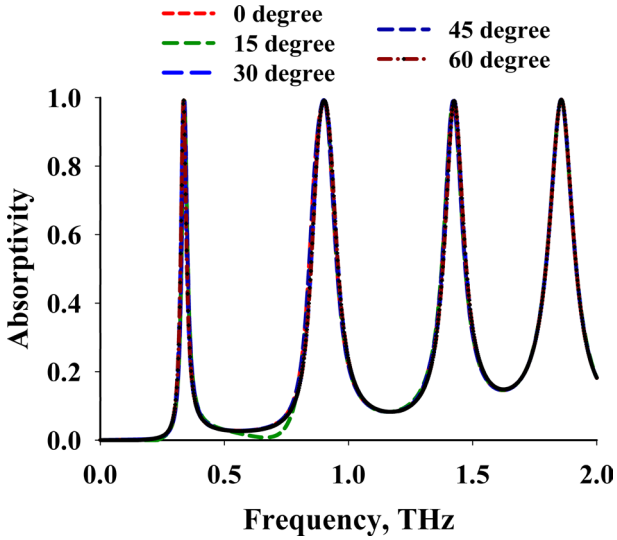

Fig. 15 Angular stability characteristics of the proposed sensor

using the refractive index property (Sharma and Sharan 2015; Islam 2018; Primo and Lebars 2007) of each of the blood components. The theoretical demonstration of the sensing capability is performed by loading the sample directly onto the surface of the THz sensor as shown in Fig. 16. This sample loading can be considered as a dielectric loading to the sensor which alters the quality factor and hence the figure of merit. The deviation in the absorption spectrum is then used as a reference to calculate the sensing performance of the proposed sensor.

The variations in the absorption characteristics of the THz sensor for various blood components are plotted in Fig. 17. From the figure, it is inferred that the absorption frequency shifts to lower frequencies with an increase in the refractive index of the blood

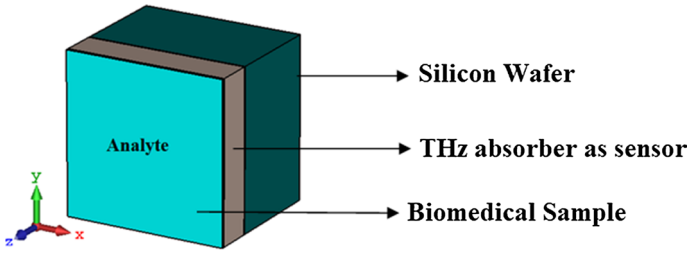

Fig. 16 Simulation setup for blood component (analyte) detection

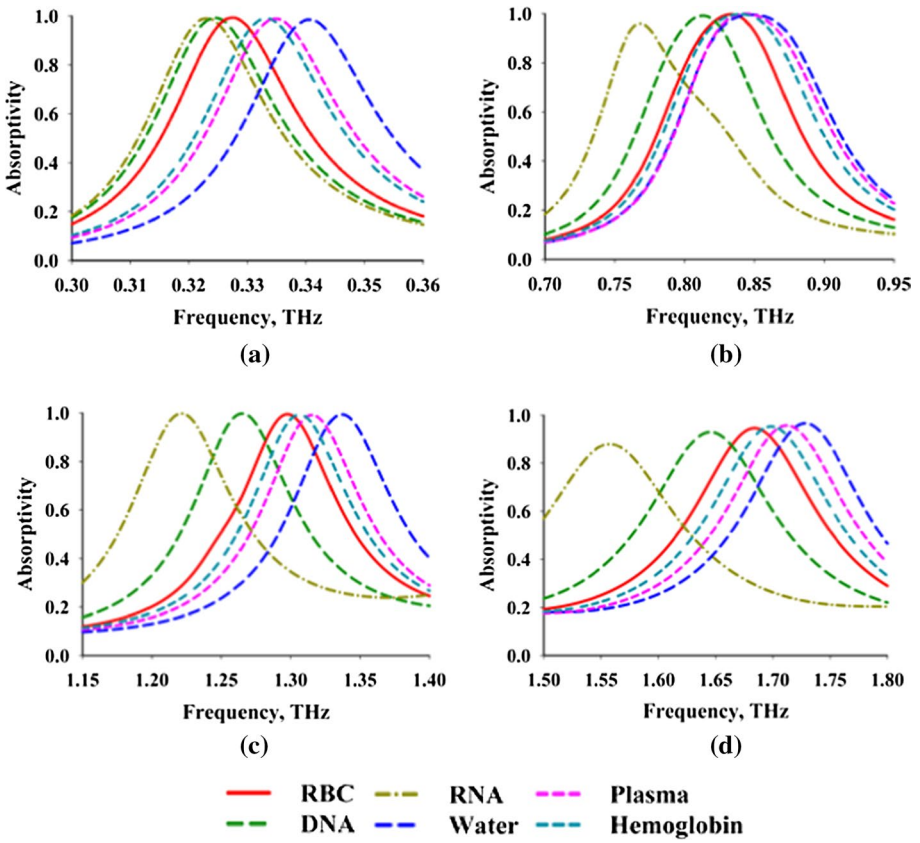

Fig. 17 Sensor performance for various components of blood at **a** 0.33 THz, **b** 0.90 THz, **c** 1.42 THz, **d** 1.85 THz

component. The estimated sensitivity of the proposed THz sensor is 10 GHz/refractive index unit (RIU) at 0.33 THz. The estimated sensitivity at second, third, and fourth absorption frequencies are 50 GHz/RIU, 66 GHz/RIU, and 102 GHz/RIU, respectively.

The refractive indices of various blood components and the corresponding sensor properties are listed in Tables 3, 4, 5 and 6 for the four absorption peaks respectively. The

Table 3 Absorption characteristics of blood components at 0.33 THz

Blood comp	N	A (%)	S, (GHz/RIU)	Δf (GHz)	FWHM (GHz)	Q	FoM
Unloaded	1	99.0	–	–	30	11	–
Water	1.33 (Islam et al. 2018)	98.8	3.48	1.15	26	12.7	0.13
Plasma	1.35 (Sharma and Sharan 2015)	98.5	2.42	0.85	26	12.7	0.09
Haemoglobin	1.38 (Sharma and Sharan 2015)	98.2	16.2	6.15	27	12.2	0.60
RBC	1.4 (Ahmed et al. 2019)	98.1	1.1	0.45	25	13.2	0.04
DNA	1.5 (Sharma and Sharan 2015)	99.3	24.08	12.04	26	12.7	0.92
RNA	1.8 (Primo and Lebars 2007)	98.2	14.2	11.35	26	12.7	0.54

Table 4 Absorption characteristics of blood components at 0.9 THz

Blood comp	N	A (%)	S, (GHz/RIU)	Δf (GHz)	FWHM (GHz)	Q	FoM
Unloaded	1	100	–	–	100	9	–
Water	1.33	99.3	170	56.1	120	7.5	1.42
Plasma	1.35	95.9	155	54.1	115	7.8	1.35
Haemoglobin	1.38	95.9	162	61.5	120	7.5	1.35
RBC	1.4	99.9	165	65.9	120	7.5	1.37
DNA	1.5	99.8	174	87.3	100	9	1.74
RNA	1.8	95.5	166	132.8	100	9	1.66

Table 5 Absorption characteristics of blood components at 1.42 THz

Blood comp	n	A (%)	S, (GHz/RIU)	Δf (GHz)	FWHM (GHz)	Q	FoM
Unloaded	1	99.0	–	–	90	15.7	–
Water	1.33	99.3	322	106.4	90	15.7	3.57
Plasma	1.35	99.3	312	109.2	100	14.2	3.12
Haemoglobin	1.38	99.3	311	118.2	94	15.1	3.31
RBC	1.4	99.2	333	133.1	100	14.2	3.33
DNA	1.5	99.4	318	159.1	100	14.2	3.18
RNA	1.8	99.7	258	206.2	90	15.7	2.87

sensitivity (S) is then measured as the ratio of frequency deviation (Δf) to change in the refractive index (Δn). From Tables 3, 4, 5 and 6, it is inferred that the proposed THz sensor offers a high sensitivity of 423 GHz/RIU for water at 1.85 THz, while the lowest sensitivity is estimated to be 1.1 GHz/RIU for RNA at 0.33 THz. Frequency deviation is tabulated as Δf (GHz) for all the blood components with respect to the unloaded biosensor. Full-Width Half Maximum (FWHM) is defined as the bandwidth of absorption at half maximum, which is estimated to be greater than 25, 100, 90, 110 GHz at four different resonant

Table 6 Absorption characteristics of blood components at 1.85 THz

Blood comp	N	A (%)	S, (GHz/RIU)	Δf (GHz)	FWHM (GHz)	Q	FoM
Unloaded	1	99.0	–	–	110	16.8	–
Water	1.33	96.0	423	139.8	140	13.2	3.02
Plasma	1.35	94.5	367	128.5	140	13.2	2.62
Hemoglobin	1.38	94.5	418	158.9	130	14.2	3.22
RBC	1.4	94.6	417	166.6	130	14.2	3.21
DNA	1.5	92.6	414	206.2	130	14.2	3.18
RNA	1.8	87.1	372	298.1	140	13.2	2.66

frequencies for most of the blood components. The Q factor is defined as the ratio of resonant frequency to FWHM. The Q factor of the proposed biosensor ranges from 7.5 to 15.7 for different blood components at the four operating bands of the biosensor. The Figure of Merit (FoM) is defined as the ratio of S to FWHM for the proposed biosensor and is calculated for all the absorption peaks corresponding to various blood components. The estimated peak FOM is 3.57 at 1.42 THz for water. The influence of the sample thickness on the sensor performance is evaluated and presented in Fig. 18. For this analysis, the average refractive index, n = 1.6, is considered. The lower absorption peak showed extremely high stability with a frequency deviation of 1 GHz/μm. The estimated frequency deviation for the second, third, and fourth absorption frequencies are 33 GHz/μm, 19 GHz/μm, and 4 GHz/μm. A comprehensive plot of the variations in the absorption peaks and the changes in the magnitude of absorptivity are plotted in Fig. 19. From the figure, it can be concluded that with an increase in refractive index, the absorption frequency decreases while the absorptivity remains greater than 85%. Table 7 presents the tolerance of ± 5% for geometrical parameters such as length of the outer square (L1), length of the outer coupled

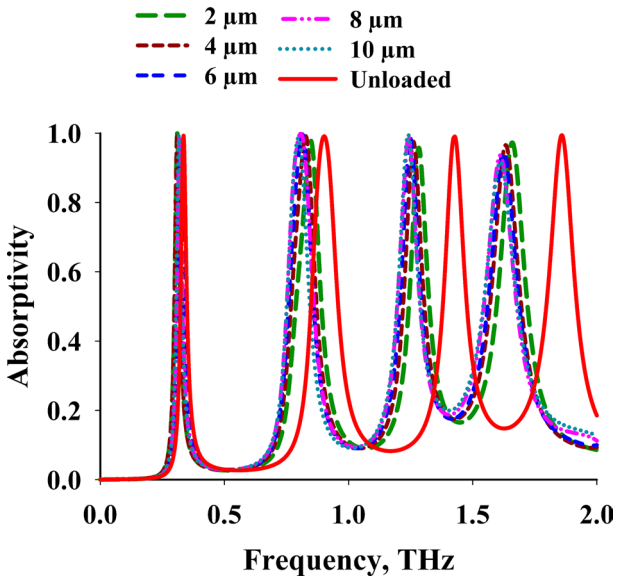

Fig. 18 Sensor performance for various sample thickness

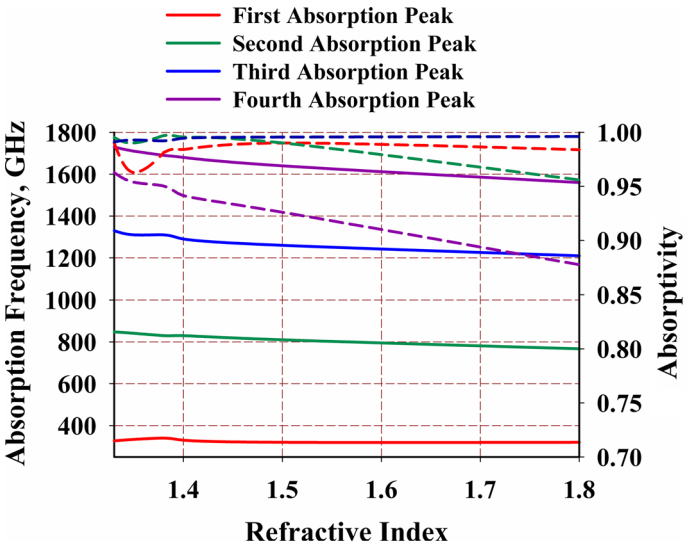

Fig. 19 Frequency deviation (solid line) and absorptivity (dotted) performance for various refractive indices

square loop (L2), and thickness of copper conductor (h4). It is inferred that a maximum deviation of 11.41% is observed for a reduction in the length of the outer coupled square loop. Thus, the absorptivity is greater than 90% for all the tolerance limits, except for the reduction in L1.

Simulation is also conducted to estimate the tolerance of the proposed sensor towards fabrication errors. The length of the outer square (L_1), the length of the outer coupled square loop (L_2) and the deposition thickness of the metallic patterns (h_4) are some of the critical parameters chosen for valuation. The deviation from the actual location of the resonant peak and the corresponding sensitivity for different cases of tolerance is evaluated and presented in Table 7. From the table, it can be inferred that the four resonant peaks can be realized with the absorptivity greater than 80% for the fabrication tolerance in the range of $\pm 5\%$. Table 8 presents a comprehensive performance comparison of the proposed sensor with other sensors reported in the literature. From the table, it can be inferred that the proposed sensor has a smaller footprint while providing high sensitivity characteristics. The proposed sensor is also characterized by four distinct operating bands which improves the overall resolution and accuracy of the sensor.

The salient features of the proposed THz sensor are,

1. The proposed THz sensor is ultra-miniaturized with the footprint of $0.164\lambda_{eff} \times 0.164\lambda_{eff}$ in comparison with (Elakkiya et al. 2019; Hu et al. 2016; Wang and Wang 2016, 2015; Ahmed et al. 2019) and (Nejat and Nozhat 2019).
2. The designed metamaterial THz sensor exhibits average peak absorption of 99.25% with four independently tunable frequency bands, viz. 0.33, 0.90, 1.42, 1.85 THz.
3. The BioMed sensor shows good angular and polarization stability.
4. The proposed sensor has selectivity at the second, third and fourth absorption peaks with good sensitivity of 10, 50, 66, 102 GHz/RIU at the respective operating bands.
5. The proposed sensor has relatively stable operating characteristics for various sample thickness with a deviation of 1, 33, 19, and 4 GHz/μm.

Table 7 Tolerance of the different geometrical parameters of the proposed bioSensor

Parameter	Tolerance (%)	Δf (THz)				% Deviation	Absorptivity for n = 1 (%)	Sensitivity (GHz/RIU)			
		0.33	0.90	1.42	1.85			330	900	1420	1850
Length of outer square (L_1)	+5	0.03	0.06	0.10	0.13	< 7.32	> 92.70	94	182	303	394
	−5	0.05	0.06	0.11	0.11	< 9.14	> 80.84	145	194	333	345
Length of the outer coupled square loop (L_2)	+5	0.02	0.06	0.09	0.13	< 7.29	> 95.19	61	179	276	409
	−5	0.03	0.10	0.13	0.10	< 11.41	> 90.18	94	318	394	306
Thickness of conductor (h_4)	+5	0.005	0.05	0.11	0.14	< 7.69	> 97.39	15	158	333	424
	−5	0.02	0.06	0.11	0.13	< 7.75	> 96.62	54	178	333	406

Table 8 Size comparison with other relevant THz unit cells

Refs.	Size ($\lambda_{eff} \times \lambda_{eff}$)	f (THz)	% Miniaturization realized with respect to reference
Hu et al. (2016)	0.437 × 0.437	1.09, 2.76, 3.23, 4.04	85.96
Wang and Wang (2016)	0.299 × 0.299	0.51, 1.25, 2.1, 2.34	70.02
Wang and Wang (2015)	0.287 × 0.287	0.92, 1.58, 2.20, 2.67, 3.33	67.43
Wang et al. 2016)	0.292 × 0.292	0.5–3	68.50
Nejat and Nozhat (2019)	0.235 × 0.141	9.40	19.03
Saadeldin et al. (2019)	0.391 × 0.391	2.25	82.46
This work	0.164 × 0.164	0.33, 0.90, 1.42, 1.85	–

5 Conclusion

This paper presented the design and characterization of a miniaturized quad-band THz sensor for BioMed applications. The proposed sensor is constructed using multi-loop resonators whose resonant frequencies can be independently controlled. A comprehensive parametric analysis was provided to tune the operating bands of the proposed sensor. The polarization and angular stability characteristics are evaluated and presented. The results indicate that the proposed sensor is polarization insensitive with angular stability up to 60 degrees with no degradation in the absorptivity. The sensitivity performance of the proposed sensor is estimated using various components of blood using the refractive indices property. The results show that the proposed sensor offers a peak sensitivity of 423 GHz/RIU at 1.85 THz. Furthermore, the effect of sample thickness on the sensitivity is analyzed and presented. From the results, it can be inferred that the proposed sensor can be used in BioMed sensing applications.

Funding This project did not receive any funding.

Availability of data and materials No new data generated and hence it is not applicable.

Code availability (Software application or custom code): The work does not involve computer code.

Declarations

Conflict of interest The authors declare that there is no conflict of interest/competing interests.

Ethical approval No human or animal subject is involved in the study. Hence not applicable.

References

Ahmed, K., et al.: Refractive index-based blood components sensing in terahertz spectrum. IEEE Sensors J. **19**(9), 3368–3375 (2019)

Al-Naib, I.: BioMedical sensing with conductively coupled terahertz metamaterial resonators. IEEE J. Sel. Top. Quantum Electron. **23**(4), 1–5 (2017)

Ansari, M.A.H., Jha, A.K., Akhter, Z., Akhtar, M.J.: Multi-band RF planar sensor using complementary split ring resonator for testing of dielectric materials. IEEE Sensors J. **18**(16), 6596–6606 (2018)

Butler, L., Wilbert, D.S., Baughman, W., Balci, S., Kung, P., Kim, S.M.: Design, simulation, and characterization of THz metamaterial absorber. In: 2011 International Semiconductor Device Research Symposium (ISDRS), College Park, MD, pp. 1–2 (2011).
CST Studio Suite Inc., www.3ds.com
Di. Primo, C., Lebars, I.: Determination of refractive index increment ratios for protein-nucleic acid complexes by surface plasmon resonance. Anal. Biochem. **368**(2), 148–155 (2007)
Elakkiya, A., Radha, S., Manikandan, E., Sreeja, B.S.: Design and numerical analysis of tri-band terahertz metamaterial. In: 2019 IEEE Region 10 Conference, Kochi, India, 2019, pp. 1922–1925.
Emami Nejad, H., Mir, A., Farmani, A.: Supersensitive and tunable nano-biosensor for cancer detection. IEEE Sensors J. **19**(13), 4874–4881 (2019)
He, S., Chen, T.: Broadband THz absorbers with graphene-based anisotropic metamaterial films. IEEE Trans. Terahertz Sci. Technol. **3**(6), 757–763 (2013)
Hu, D., Wang, H., Tang, Z., et al.: Design of four-band terahertz perfect absorber based on a simple #-shaped metamaterial resonator. Appl. Phys. A **122**, 826 (2016)
Islam, M.S., et al.: A novel approach for spectroscopic chemical identification using photonic crystal fiber in the terahertz regime. IEEE Sensors J. **18**(2), 575–582 (2018)
Landy, N.I., Sajuyigbe, S., Mock, J.J., Smith, D.R., Padilla, W.J.: Perfect metamaterial absorber. Phys. Rev. Lett. **100**, 207402 (2008)
Landy, N.I., Bingham, C.M., Tyler, T., Jokerst, N., Smith, D.R., Padilla, W.J.: Design, theory, and measurement of a polarization-insensitive absorber for terahertz imaging. *Phys. Rev. B*. 79 (2009).
MacPherson, E., Gallerano, G.P., Park, G.-S., Hintzsche, H., Wilmink, G.J.: Guest editorial: terahertz imaging and spectroscopy for biology and BioMedicine. IEEE J. Biomed. Health Inform. **17**(4), 765–767 (2013)
Nagel, M., Richter, F., Bolivar, P.H., Kurz, H., Bosserhoff, A., Buttner, R.: Integrated THz biomolecular sensors for DNA. In: Proceedings, IEEE 10th International Conference on Terahertz Electronics, Cambridge, UK, pp. 70–73 (2002).
Nejat, M., Nozhat, N.: Ultrasensitive THz refractive index sensor based on a controllable perfect MTM absorber. IEEE Sensors J. **19**(22), 10490–10497 (2019)
Nejat, M., Nozhat, N.: Multi-band MIM refractive index biosensor based on Ag-air grating with equivalent circuit and T-matrix methods in the near-infrared region. Sci. Rep. **10**, 6357 (2020)
Saadeldin, A.S., Hameed, M.F.O., Elkaramany, E.M.A., Obayya, S.S.A.: Highly sensitive terahertz metamaterial sensor. IEEE Sensors J. **19**(18), 7993–7999 (2019). https://doi.org/10.1109/JSEN.2019.2918214
Sanphuang, V., Yeo, W., Volakis, J.L., Nahar, N.K.: THz transparent metamaterials for enhanced spectroscopic and imaging measurements. IEEE Trans. Terahertz Sci. Technol. **5**(1), 117–123 (2015)
Sharma, P., Sharan, P.: Design of photonic crystal based ring resonator for detection of different blood constituents. Opt. Commun. **348**(08), 19–23 (2015)
Shi, C., et al.: Compact broadband terahertz perfect absorber based on multi-interference and diffraction effects. IEEE Trans. Terahertz Sci. Technol. **6**(1), 40–44 (2016)
Tao, H., et al.: Highly flexible wide angle of incidence terahertz metamaterial absorber: Design, fabrication, and characterization. Phys. Rev. B **78**, 241103 (2008)
Wang, G., Wang, B.: Five-band terahertz metamaterial absorber based on a four-gap comb resonator. J. Lightw. Technol. **33**(24), 5151–5156 (2015)
Wang, B., Wang, G.: Quad-band terahertz absorber based on a simple design of metamaterial resonator. IEEE Photon. J. **8**(6), 1–8 (2016)
Wang, B., Wang, G., Zhai, X., Wang, L.: Polarization tunable terahertz metamaterial absorber. IEEE Photon. J. **7**(4), 1–7 (2015)
Wang, B., Wang, G., Wang, L., Zhai, X.: Design of a five-band terahertz absorber based on three nested split-ring resonators. IEEE Photo. Technol. Lett. **28**(3), 307–310 (2016)
Wang, B., Xie, Q., Dong, G., Huang, W.: Simplified design for broadband and polarization-insensitive terahertz metamaterial absorber. IEEE Photon. Technol. Lett. **30**(12), 1115–1118 (2018)
Wang, Z., et al.: Characterization of thin metal films using terahertz spectroscopy. IEEE Trans. Terahertz Sci. Technol. **8**(2), 161–164 (2018)
Wilbert, D.S., Hokmabadi, M.P., Kung, P., Kim, S.M.: Equivalent-circuit interpretation of the polarization insensitive performance of THz metamaterial absorbers. IEEE Trans. Terahertz Sci. Technol. **3**(6), 846–850 (2013)